In-situ growth of ultrathin Co-MOF nanosheets on α-Fe$_2$O$_3$ hematite nanorods for efficient PEC water oxidation

Qi Zhang [a], Hongyan Wang [a,*], Yixin Dong [a], Xuebin Ke [b], Quanping Wu [a], and Song Xue [a,*]

[a] *Tianjin Key Laboratory of Organic Solar Cells and Photochemical Conversion, School of Chemistry & Chemical Engineering, Tianjin University of Technology, Tianjin, 300384, China;*

[b] *School of Engineering and Computer Science, University of Hull, Hull, HU67RX,UK*

Corresponding author: Fax: +86-22-60214252; E-mail address: wanghongyan12@hotmail.com; xuesong@ustc.edu.cn.

Abstract:

Efficient charge transport is a key factor for photoelectrochemical (PEC) water splitting. The charge transfer at the semiconductor/electrolyte interface is of paramount importance especially for the complex water oxidation reaction. Here, we explored the feasibility of improving the charge transfer at the semiconductor/electrolyte interface by in-situ growth of Co-MOFs through a facile ion-exchanging method. Under optimized conditions, the Co-MOF nanosheets modified hematite gave a photocurrent density of 2.0 mA cm^{-2} at 1.23 V $_{RHE}$ with a cathodic shift of 180 mV in the photocurrent onset potential, relative to bare α-Fe$_2$O$_3$. To elucidate the role of Co-MOF, X-ray photoelectron spectroscopy (XPS), electrochemical impedance spectroscopy (EIS) and Mott-Schottky (M-S) measurements were carried out. It is found that the uniformly distributed Co^{2+} in Co-MOF possessed excellent hole storage capability and charge transfer efficiency evidenced by the high surface capacitance and extremely low surface charge transfer resistance. Moreover, the in-situ formed Co-MOF showed higher concentration of unsaturated Co-N$_x$ than that of powder formed ZIF-67, which facilitated O species chemisorption and accordingly acted as highly active centers for water oxidation.

1. Introduction

Solar energy conversion using a photoelectrochemical (PEC) water splitting system has been considered as one of the strategies to solve the global energy problems [1, 2]. As the most important component in a PEC system, semiconductor photoelectrodes have attracted numerous attentions [3, 4]. Hematite (α-Fe$_2$O$_3$) has been extensively studied as one of the most promising photoanonde materials for water splitting due to its low toxicity, ample abundance, appropriate band edge position and high chemical stability [5, 6].

With a band gap of 2.1 eV, Fe$_2$O$_3$ has a theoretical solar-to-hydrogen efficiency (STH) of 16.8% under AM 1.5G irradiation [7]. However, it is difficult to reach the theoretical value due to several limitations. One of the major problems preventing its practical application is the sluggish water oxidation kinetics in the interface of semiconductor/electrolyte. Normally, a large applied potential is needed to produce a photocurrent. In order to reduce the required applied potential, exploring highly efficient catalyst is of significant demand. Noble metal oxides of ruthenium/iridium are the most active oxygen evolution catalyst for the low overpotential and large current density [8]. However, they suffer from high cost and poor durability, which hinders the application of these materials. To solve this problem, many studies have been carried out to develop highly efficient and low-cost OER catalyst, such as developing transition metal compound [9-13]. Especially, cobalt-based materials turn to be promising alternatives to replace noble metal oxides, namely CoO$_x$, cobalt phosphate catalyst "Co-Pi" [14-17]. Since the catalytic process only occurs on the surface of catalysts, it is essential to downsize Co-based species with more catalytic active sites exposed [18].

Seen from this perspective, Co-based MOF seems to be an ideal candidate, in which Co centers are atomically distributed. For example, a cobalt–containing catalyst (Co-ZIF-9) worked effectively for the electrochemical oxygen evolution reaction. By theoretical calculation, this catalyst was found be capable of activating the water molecule via binding the OH- group to the metal sites with low activation barriers, while the eliminated proton was accepted by the nearby benzimidazolate motifs [19]. Recently, another Co-based MOFs, zeolitic imidazolate frameworks-67 (ZIF-67) have

also been studied intensively for their electrocataltyic activities in OER. But intrinsically, ZIF-67 shows poor catalytic activity for OER [20]. In principle, Co ions in the bulk ZIF-67 are coordinated by four strong imidazole ligands without available sites for adsorption and thus for electrocatalysis [21]. However, some successful attempts were made. For example, coordinatively unsaturated metal sites (CUMS) were created by removing some of the ligands using dielectric barrier discharge plasma etching. The CUMSs in ZIF-67 acted as excellent catalytic centers for OER with a promising electrocataltyic activity [22]. In another study, active atomic–scale CoO_x species were obtained when O_2 plasma was used, which is found to be the active sites to catalyze the oxygen evolution reaction [20]. Xu *et al* [23] fabricated Ti@TiO_2 nanowire supported ZIF-67 electrode through electrodeposition and self-sacrificial template strategy, which showed enhanced OER with a small Tafel slope (42 mV/dec) and overpotential (0.41V) at the current density of 10 mAcm^{-2}.   So far, the literature on enhancing the photo-electrocatalytic activity of photoanodes (e.g. hematite) with Co-based MOF as co-catalyst remains scarce, though these are attractive possibilities.

Herein, we explored the feasibility of improving the charge transfer in the interface of hematite photoanodes and electrolyte by in-situ growth of Co-MOFs through a facile ion-exchanging method. Co $(NO_3)_2$ and 2-methylimidazole were used as precursors for in-situ growth of Co-MOF. Co^{2+} nodes were linked through N atoms by 2-methylimidazole groups. When Co^{2+} interacts with 2-methylimidazolate, the electronegative N atom can serve as an electron sink, which is beneficial for the formation of Co ions with higher valence state [24]. Since the metal carries highly positive charges, it strongly interacts with oxygen, facilitating O species such as OH, OOH reversible chemisorption and acting as OER active centers. The atomically distributed Co^{2+}on the surface of hematite is expected to store the photo-generated holes effectively and transfer to the electrolyte efficiently.

2. Experimental section

2.1. Materials preparation

(a) Preparation of bare hematite films

The pristine hematite films on conductive glass substrate were synthesized through a simple solution-based method. In a typical process, a clean FTO (F:SnO$_2$) glass was put into a 10-mL beaker containing a 4mL solution of 0.0972g FeCl$_3$·6H$_2$O (0.09M) and 0.034g NaNO$_3$ (0.1M) at pH=1 adjusted by HCl. Next, the 10mL vial containing the above solution and FTO glass was carefully placed into the 100mL Teflon-lined autoclave. After hydrothermal reaction was conducted at 95 °C for 4 h, a uniform layer of FeOOH film was formed on the FTO substrate. The substrates were thoroughly rinsed with distilled water and then dried in air. The FeOOH film was annealed at 550°C for 2hs and 750°C for 15min in air, followed by natural cooling to room temperature to give bare hematite film.

(b)Preparation of Co modified hematite photoanodes

To prepare Co modified hematite films, a series of bare hematite were prepared first for further modification. In a typical synthesis, 58mg of Co(NO$_3$)·6H$_2$O（0.1M） was dissolved in 2mL of deionized water. Those as-synthesized bare hematite films were spin-coated with 100uL of the as-prepared Co(NO$_3$)·6H$_2$O aqueous solution at 1200 rmp for 12s, Then, the surface-treated samples were subjected to heat at 70°C for 20min. The resultant samples were referred to as Fe$_2$O$_3$@0.1Co.

(c) Preparation of MIm (2-methylimidazole) modified hematite photoanodes.

For MIm modified hematite photoanodes, the as-synthesized bare hematite films were immersed into 4 mL of 2-methylimidazole aqueous solution（0.8M）for 20 min and washed with distilled water. Then, the surface-treated samples were subjected to heat at 70°C for 20min. The resultant samples samples were referred to as Fe$_2$O$_3$@0.8 MIm.

（d）Preparation of Co-MOF modified hematite photoanodes

To prepare in-situ Co-MOF modified hematite photoanodes，the Co modified hematite film (such as Fe$_2$O$_3$@0.1Co) were immersed into 4 mL of 2-methylimidazole aqueous solution（0.8M）for 20 min and washed with distilled water. Then, the surface-treated samples were subjected to heat at 70°C for 20min. The resulted samples were referred to as Fe$_2$O$_3$@0.1Co@0.8MIm, where "0.1Co" and "0.8MIm" means that the

0.1M $Co(NO_3)\cdot 6H_2O$ and 0.8M MIm precursor solutions were used. Varied concentration of $Co(NO_3)_2$ (0.05M,0.1M,0.2M) and 2-methylimidazole (0.4M,0.8M,1.6M) were used, and the as-prepared samples were referred to as Fe_2O_3@0.05Co@0.8MIm Fe_2O_3@0.05Co@0.8MIm, Fe_2O_3@0.1Co@0.8MIm, Fe_2O_3@0.2Co@0.8MIm, Fe_2O_3@0.1Co@0.4MIm and Fe_2O_3@0.1Co@1.6MIm and etc.

2.2. Materials characterisation

The crystal structures of the samples were characterised by X-ray powder diffraction (XRD) with a Rigaku D/MAX-2500 powder diffractometer (Japan) using Cu Kα radiation ($\lambda = 0.154\ 18$ nm) and an accelerating voltage of 30 kV and emission current of 20 mA. Scanning electron microscopy (SEM) with energy dispersive spectrometer (EDS) was carried out on a JEOL/JSM7500 to characterise the surface morphology and element distribution in the films. X-Ray photoelectron spectroscopy (XPS) was performed on an ESCALAB-250XI spectrometer (Thermo Fisher Scientific，USA) with monochromated Al Kalph (150W) as the X-ray source for excitation. The optical properties of the α-Fe_2O_3 films were obtained using a UV-visible spectrophotometer (Shimadzu, UV-2600), and $BaSO_4$ was used as a reference.

2.3 Photoelectrochemical measurements

The photoelectrochemical experiments were conducted in a glass cell using a 300-W xenon lamp. The light power density (100 mW cm^{-2}) at the position of the sample was measured with a power meter (TYD, FSR-2). The electrochemical properties of the hematite samples were investigated with a Zennium electrochemical workstation (ZAHNER, Germany) using a three-electrode system with the as-prepared sample as the working electrode, platinum wire (99.9%) as the counter electrode, and an Ag/AgCl (saturated KCl) electrode as the reference electrode in a 1.0 M NaOH electrolytic solution at room temperature. All potentials were converted to the reversible hydrogen electrode (RHE) scale using the equation $V_{RHE} = V_{Ag/AgCl} + 0.1976$ V + pH (0.059 V). Mott-Schottky (M-S) measurements were performed in a dark condition at 1 kHz frequency in 1M NaOH electrolyte solution with the same three electrode configuration. The electrochemical impedance spectroscopy (EIS) was carried out under light

irradiation with 0.05V bias against reference electrode of Ag/AgCl in an aqueous solution containing 0.5M KCl, 0.01M $K_3[Fe(CN)_6]$ and 0.01M $K_4[Fe(CN)_6]$ using the same three electrode system.
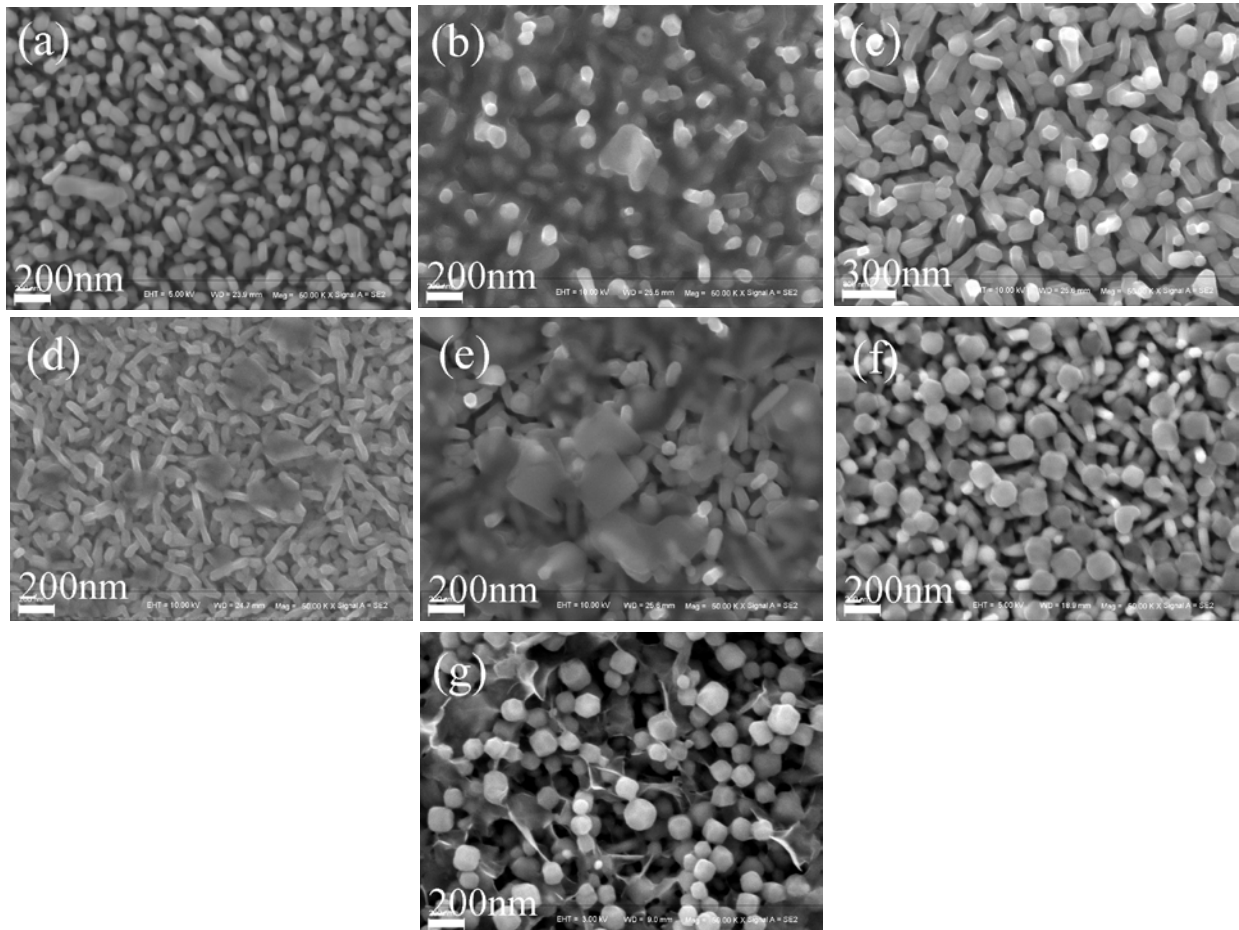
3. Results and discussion:

Fig.1 SEM micrographs of hematite (a) and surface modified Fe_2O_3 with varied Co/MIm ratios: (b) $Fe_2O_3@0.1Co$ (c) $Fe_2O_3@0.8MIm$ (d) $Fe_2O_3@0.05Co@0.4$ MIm (e) $Fe_2O_3@0.1Co@0.8MIm$ (f) $Fe_2O_3@0.2Co@1.6$ MIm (g) $Fe_2O_3@0.3Co@2.4MIm$

The morphology and structure of the samples were analyzed by scanning electron microscopy (SEM) and transmission electron microscopy (TEM). Fig. 1 gives the top-view SEM images of bare hematite and α-Fe_2O_3 treated with MOF precursors. As shown in Fig. 1a, nanorod arrays generally grow vertically to the FTO substrate for bare Fe_2O_3. For comparison, the precursors of Co based MOF, including $Co(NO_3)_2$, 2-

methylimidazole were deposited on bare hematite films alone or together. As shown in Fig.1b, the samples spinning-coated with Co (NO$_3$)·6H$_2$O was covered with layers of gel-like CoOx crystallites which filled into the clearance between the nanorods of hematite. While, for 2-methylimidazole soaked samples (Fig.1c), there is little morphology changes, which is probably due to the limited amount of 2-methylimidazole absorbed. However, for the samples treated with Co (NO$_3$)$_2$ and 2-methylimidazole consecutively, Co-based MOF nano-sheets (200-300nm in square) were formed and loosely dispersed on the surface of hematite (Fig.1d). Then, by increasing the concentrations of both Co (NO$_3$)$_2$ and 2-methylimidazole, more nano-sheet structured MOF with larger size were observed on the surface of hematite (Fig.1e). However, further increasing the concentration of the MOF precursors, smaller particles with polyhedron shape were formed and aggregated on the top of hematite nanorods (Fig.1 f,g).
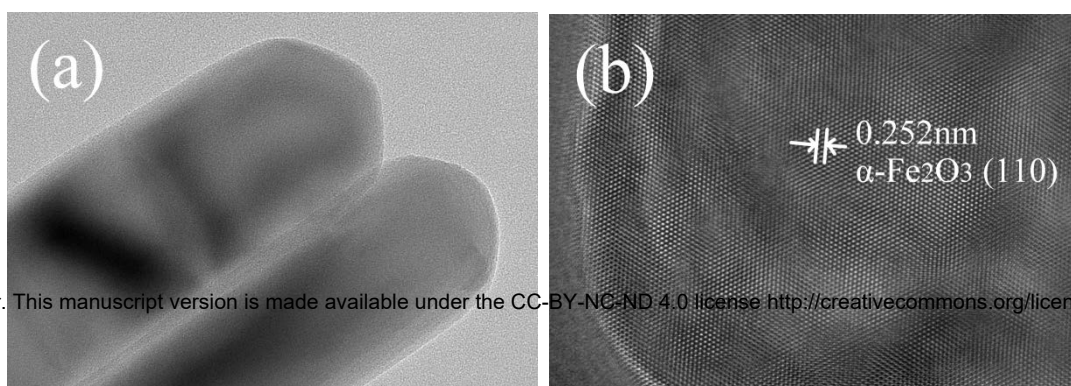
0.252nm
α-Fe$_2$O$_3$ (110)

Fig.2 a, b) TEM micrographs of bare hematite; c, d) TEM micrographs of Fe$_2$O$_3$@0.1Co@0.8MIm; e, f, g) EELS images of Fe$_2$O$_3$@0.1Co@0.8MIm

The transmission electron microscopy (TEM) and electron energy loss spectroscopy (EELS) for the samples Fe$_2$O$_3$@Co-based MOF and bare hematite are shown in Fig. 2. Electron energy loss spectroscopy (EELS) is a technique usually mounted on a transmission electron microscope that is especially suited to the characterization of light elements which are difficult to deal with EDS. TEM image in Fig.2a confirm the nanorod structure of the hematite. The HRTEM image of the bare hematite shown in

Fig.2b clearly reveals lattice fringes with d-spacing values of 0.252 nm, which can be indexed to the α-Fe$_2$O$_3$ (110) crystal plane.

However, seen from the HRTEM image of the sample α-Fe$_2$O$_3$/0.1Co/0.8MIm (Fig.2d), the surface of hematite has been partially covered by amorphous layers of Co-based coordination polymer.   A few lattice fringes of α-Fe$_2$O$_3$ in the uncovered areas still can be observed. Furthermore, it can be seen clearly from the EELS images (Fig.2e-g) that, cobalt and nitrogen (2-methylimidazole) elements are uniformly distributed over the hematite nanorod. Combining with the SEM images, it can be inferred that besides the nano-sheet or polyhedron structured Co-based MOF on the top of the hematites, amorphous Co coordination polymer may also exist on the surface of the hematite naorods.

The hematite films deposited with Co-based MOF films were further characterized with XRD analysis. As shown in Fig. S1, compared with the spectra of FTO substrate, two additional diffraction peaks at 35.6^o and 64.2^o were clearly observed in all the hematite thin films, which could be assigned to the (110) and (300) planes of α-Fe$_2$O$_3$, respectively. No others peaks were observed in all those samples, which is probably due to the limited amount and scattered arrangement of the MOF particles. Instead, higher amount of Co-MOF powder were prepared in a similar procedure: 0.1M Co (NO$_3$)·6H$_2$O and 0.8 M 2-methylimidazole solutions were mixed, followed by centrifugation and washing.   As shown in Fig. S2, the XRD peaks of the Co-MOF powder particles match well with the simulated ZIF-67 peaks published in the literature [25]. Moreover, the optical properties of the surface modified α-Fe$_2$O$_3$ films were measured using a UV-visible spectrophotometer. As seen in Fig S3. 4, similar absorbance spectra were observed for surface modified samples, indicating that the film thickness and light absorbance were not affected by the surface modification.
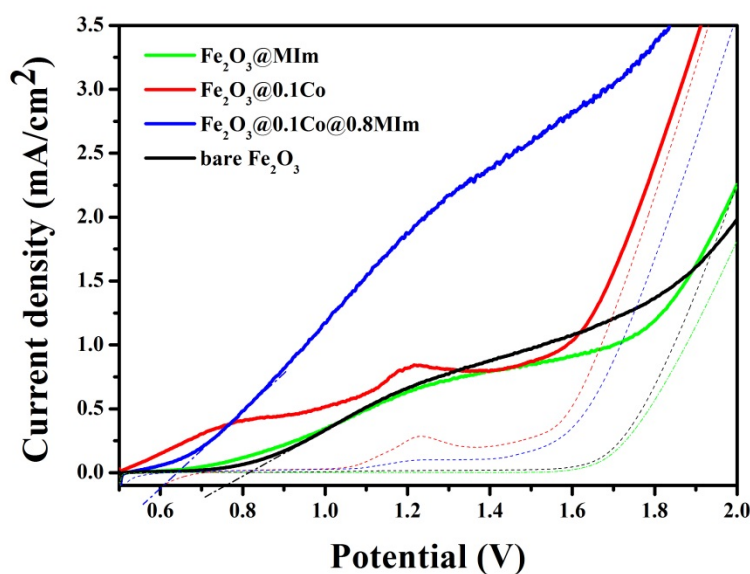
Fig.3 *J-V* characteristics curves of bare and surface modified hematite films were recorded in 1.0 M NaOH in the dark (dashed lines) and under light illumination (solid lines).

The current-voltage (*J-V*) curves of the as-prepared bare and surface modified hematite films were recorded in the dark and light illumination as shown in Fig.3. A photocurrent of 0.71 mA cm^{-2} was recorded for the bare Fe_2O_3 at +1.23 V_{RHE}. The *J-V* curve of the Fe_2O_3@MIm resembled that of the bare hematite photoanodes very closely, indicating that a thin layer of organic linkers may not affect the surface characteristic much. Instead, surface treatment with Co $^{2+}$ yielded a cathodic shift of 260 mV in the photocurrent onset potential relative to bare α-Fe_2O_3. Besides, an obvious photocurrent peak appeared at about 1.2 V vs RHE. A similar peak was also observed for the sample Fe_2O_3@Co 0.1 in the dark condition, indicating that it is the oxidation peaks of Co (II) ions on the surface of hematite. Further deposition with 2-methylimidazole ligand (Fe_2O_3@Co0.1@MIm0.8) led to a significant improvement in the photocurrent density, up to 2.0 mA cm^{-2} at 1.23 V_{RHE} with a cathodic shift of onset potential from 0.82 to 0.64 V_{RHE}. Meanwhile, the Co 2+/3+ oxidation peaks have been greatly suppressed both in the dark and illumination conditions. Normally, when Co^{2+} interacted with imidazole ligands, most of the Co ions are fully coordinated with four electronegative N atoms (except for those on the surfaces)[22]. In such case, Co^{2+}

oxidation reaction is likely to be restrained due to the electronic coupling effects between the Co and organic linkers.

The onset potential of dark current can provide information as to electrocatalytic activity of water oxidation on the Fe_2O_3 electrode [26]. Compared with bare α-Fe_2O_3, the dark onset potential of Co treated Fe_2O_3 exhibited considerable cathodic shifts. Generally, a lower dark current onset potential indicates higher electrocatalytic activity for water oxidation [27]. This indicates that the surface treatment with Co species makes the electrode more catalytic for O_2 evolution which has been widely observed in many cobalt based catalyst such as cobalt phosphate (Co-Pi)[9, 28, 29] and cobalt oxide [30-32]. In this study, the assembly of cobalt ions and the 2-methylimidazole was conducted in a facile method. Co ions and 2-methylimidazole were deposited on the hematite surface separately to in-situ grow well dispersed Co-MOF nanosheets. The porous Co-MOF contains abundant Co active site which may act as fast redox mediators to facilitate the photoelectrochemical water oxidation.
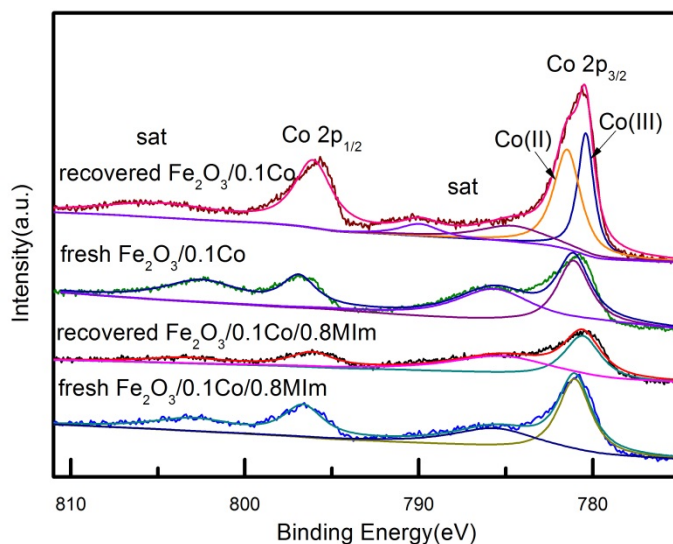

Fig.4 High resolution Co 2P spectra of Fe_2O_3@0.1Co and Fe_2O_3@0.1Co@0.8MIm before and after reactions

To check the surface characteristics changes of the samples before and after the reaction, XPS measurements were conducted for the fresh and used samples. The high resolution Co 2p XPS spectrums for Co and Co-MOF modified hematite photoanodes

were shown in Fig.4. For the fresh catalyst, the Co 2p XPS spectrum can be deconvolved into four peaks, corresponding to Co $2p_{1/2}$, Co $2p_{3/2}$ fitting peaks at 796.9, 781.1eV respectively, as well as their shakeup satellites (denoted as "sat"), implying the existence of CoO in the Fe_2O_3@0.1Co [33-35]. After further deposition with 2-methylimidazole ligand, slight shift was obtained for the Co $2p_{1/2}$, Co $2p_{3/2}$, due to different electronegativelity of N (MIm) and O (CoO) [23]. After PEC reaction, the Co $2p_{1/2}$ and Co $2p_{3/2}$ peaks of sample Fe_2O_3@0.1Co@0.8MIm slightly shifted to lower values of binding energies, which can be ascribed to the adsorption of OH, OOH species and slightly partial oxidation of Co (II) during the reaction. However, for sample Fe_2O_3@0.1Co，the shape and position of the Co $2p_{1/2}$ and Co $2p_{3/2}$ peaks have been greatly changed after the reaction. Compared with fresh Fe_2O_3@0.1Co, a smaller spin-orbit splitting $\Delta E(2p_{1/2} - 2p_{3/2})$, a narrower FWHM and lower values of binding energy were observed for the used sample, which is a typical character for the existence of Co (III) [36, 37]. This is consistent with results observed in the *J-V* curves of bare and surface modified hematite films (Fig.3)
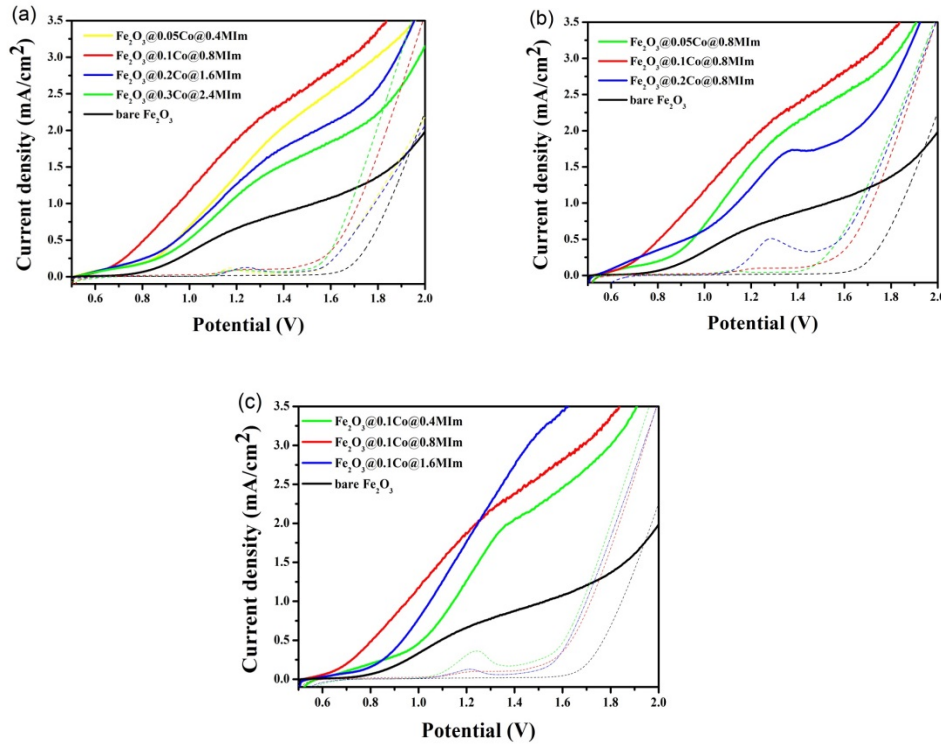

Fig.5 *J-V* characteristics curves of bare and surface modified hematite films with varied

Co/MIM ratios were recorded in 1.0 M NaOH in the dark (dashed lines) and under light illumination (solid lines).

Varied Co/MIm ratios have also been attempted to prepare the Fe_2O_3@Co-MOF photoanodes and the *J-V* curves of the bare and surface modified hematite films were recorded in the dark and light illumination (Fig.5). As shown in Fig.5a, the Co/MIm ratios have been kept constant (Co/MIm=0.1/0.8), while changing the amount of Co and 2-methylimidazole simultaneously. Their corresponding SEM micrographs have been shown in Fig.1 d - f, respectively. In Fig.5b, the amount of 2-methylimidazole was kept constant (0.8M), while changing the amount of Co. Similarly, the amount of Co remain to be 0.1M with varied amount of 2-methylimidazole (Fig.5c). Based on the above plots, it can be inferred that the more Co, the lower onset potential, and the larger Co (II) oxidation peak was observed in the light and dark current (Fig.5b). However, the Co (II) oxidation peak can be effectively suppressed by addition of 2-methylimidazole. Furthermore, it is worth mentioning that at 1.2<E<1.7 V, the photocurrent slope of the Fe_2O_3/0.1Co/0.8MIm decreased, suggesting a decrease in the O_2 evolution rate (Fig5c). Actually, 1.1 V_{RHE} corresponds to the potential where Co oxidation states are activated (see Fig.3 and Fig.5). In the Co-MOF modified sample, holes that reach surface traps may be transferred to the surface bound catalyst and injected into the electrolyte. At low potential this process is more effective, while for 1.2<E<1.7 V, some transient holes present in the Co-MOF layer may be scavenged into the oxidation cycle of Co(II)→Co(III), reducing the positive effect of the electrocatalyst. For the sample with higher content of MIm, such as Fe_2O_3/0.1Co/1.6 MIm, the side effects were weakened due to the coordination effect of organic ligands. Therefore, Fe_2O_3/0.1Co/1.6 MIm showed a steeper photocurrent slope in a wider voltage range (Fig5c).

To further elucidate the role of Co-MOF, electrochemical impedance spectroscopy (EIS) was applied to samples of bare and surface modified α- Fe_2O_3. The Nyquist plot measured under illumination for bare and surface modified hematite electrodes at 1.05V_{RHE} can been in Fig. 6a.　The spectra consisted of two overlapping semicircles,

and the low frequency (high impedance) semicircle was clearly much smaller for all the Co-MOF deposited hematite (Fe_2O_3@0.1Co@0.8MIm) compared to the bare electrode. The Co or MIm modified sample showed similar profiles as that of the bare hematite. A general equivalent circuit, EC, was used to interpret the EIS data as shown in the inset of Fig. 6a. The proposed circuit consisted of all the series resistances in the electrochemical cell, R_s , the capacitance of the bulk hematite, C_{bulk}, charge transfer resistance from the valence band of the hematite, $R_{ct,bulk}$, a capacitance of the surface state, C_{ss}, and charge transfer resistance from the surface states, $R_{ct,ss}$. Hamann *et al* conducted a detailed investigation on photoelectrochemical impedance spectroscopy of "Co-Pi" coated hematite electrodes [38]. It was found that C_{ss} increased with thickness of "Co-Pi", which was consistent with the assignment of this capacitance to the chemical capacitance of "Co-Pi". Combining the results of transient anodic/cathodic photocurrent and EIS, it clearly showed that C_{ss} can provide direct and clear evidence of hole storage throughout the surface "Co-Pi" film [10, 38]. In our case, the C_{ss} accounts for the hole storage capability throughout the surface of hematite. The fitting results for the Nyquist plots have been summarized in Table S1 (ESI). The highest C_{ss} values was obtained for sample Fe_2O_3@0.1Co@0.8MIm, indicating a highest hole storage capability due to the Co-MOF layers. It's worth mentioning that, compared with bare hematite ($R_{ct,ss}$ =107.2 Ωcm^2), Fe_2O_3@Co-MOF possessed extremely low surface charge transfer resistance ($R_{ct,ss}$=13.5 Ωcm^2). This is consistent to an earlier report that the interfacial charge transfer (water oxidation) is related to the charging of these surface states [38, 39]. The hole transfer step leading to water oxidation takes place predominantly from surface trapped holes and not directly from holes in the valence band[39]. Therefore, a larger number of trapped holes in the Co-MOFs (C_{ss}) implied higher density of active sites readily for water oxidation, which indicated faster interfacial charge transfer (lower $R_{ct,ss}$)[40].
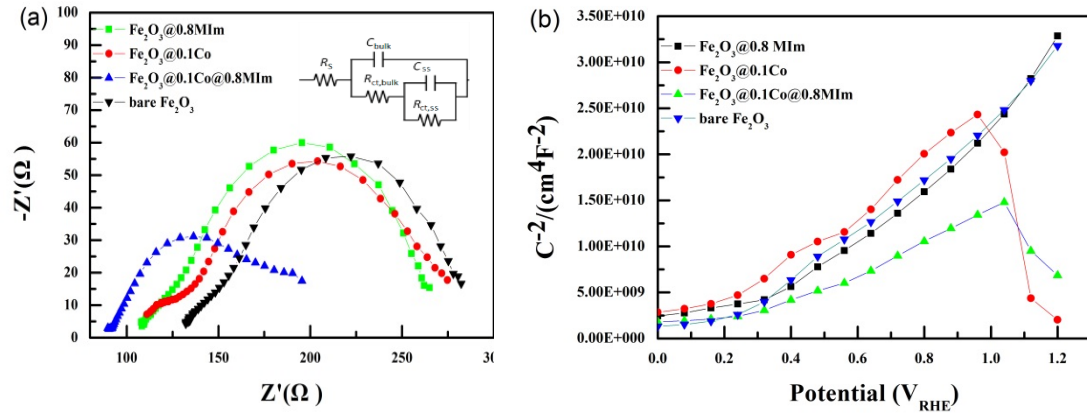
Fig.6. (a) EIS results and (b) Mott-Schottky plots of bare α-Fe$_2$O$_3$, and surface modified α-Fe$_2$O$_3$ films

To better understand the electronic effect of surface Co-MOF on the hematite, we carried out Mott-Schottky (M-S) measurements in the dark in the potential range from 0-1.2 Vvs RHE. (Fig.6b). The bare electrode (black squares, Fig.6b) showed a positive slope, indicating that α-Fe$_2$O$_3$ is an n-type semiconductor with the electrons being the majority carriers. However, it was found that the Co containing samples, such as Fe$_2$O$_3$@Co and Fe$_2$O$_3$@0.1Co@0.8 MIm, exhibited concomitant presence of positive and negative slopes. The curves of the Co modified samples changed slope above 1.0 V, corresponding to the redox activity of Co, which led to an altered electronic behavior. The slopes determined from the M-S plots were used to estimate the carrier densities using the following M-S equation as presented in Fig.6b:

$$\left(\frac{A_S}{C_{CS}}\right)^2 = \frac{2}{e\varepsilon\varepsilon_0 N_D}(V - E_{fb} - \frac{kT}{e})$$

where A_S is the real surface area of the electrode, C_{CS} is the space charge capacitance, e is the elementary charge, ε is the dielectric constant of hematite, ε_0 is the permittivity of vacuum (8.854×10^{-14} C V^{-1} cm^{-1}), V is the applied potential, k is Boltzmann's constant, E_{fb} is flat-band potential and T is the absolute temperature. As shown in Fig.6b, the presence of Co-MOF significantly decreased the slope of the M-S plot, indicating the increasing electron density ($N_d=1*10^{20}$ cm^{-3}) of Fe$_2$O$_3$@Co0.1@0.8MIm,   as

relative to bare Fe_2O_3 ($N_d = 6.2*10^{19} cm^{-3}$).

Scheme 1 shows the proposed mechanism of the PEC water oxidation on Co-MOF modified hematite photoanodes. Those in situ formed Co-MOFs nanosheets did not show a well crystallized structure as the power formed ZIF-67. In principle, Co ions in the bulk of ZIF-67 are coordinated by four strong imidazole ligands without accessible sites for adsorption and thus catalysis. So, to study the Co coordination geometry, the chemical state of Fe_2O_3@Co0.1@0.8MIm and pristine ZIF-67 were dected by XPS. Fig. S6 shows the Co 2p XPS spectra of the two samples. Compared to that in pristine ZIF-67, the Co 2p XPS peak in Fe_2O_3@Co0.1@0.8MIm showed a significant broadening, indicating the change of the coordination geometry of Co ions. To confirm this change, The Co 2p peaks in both samples were carefully deconvoluted. The Co 2p $_{3/2}$ of ZIF-67 was deconvoluted into four components. The peak at 781.9 eV is attributed to fully coordinated cobalt with the $Co-N_4$ environment, and the peak at 780.6 eV is attributed to the unsaturated cobalt species in Co-Nx (x<4) geometry [22, 41]. The unsaturated Co species in the pristine ZIF-67 mainly locate on the external surface or the in-situ formed defect sites during its synthesis [21]. The other two peaks are satellite peaks. The Co 2p XPS peak in the Fe_2O_3@Co0.1@0.8MIm could also be deconvoluted into the similar four peaks. However, the cobalt species in $Co-N_x$ geometery significantly increased, indicating more coordinatively unsaturated cobalt species Co-N_x (x<4) existing in the Co-MOF nanosheets. In another word, higher percentages of exposed catalytic active surfaces existed in surface of the Fe_2O_3@Co0.1@0.8MIm. Those unsaturated cobalt species strongly interacts with oxygen, facilitating O species such as OH, OOH reversible chemisorption and accordingly acting as highly active centers for water oxidation as depicted in Scheme 1.

H_2O

$Co-N_x$

$Co^{2+} \longleftrightarrow Co^{3+}$

O_2
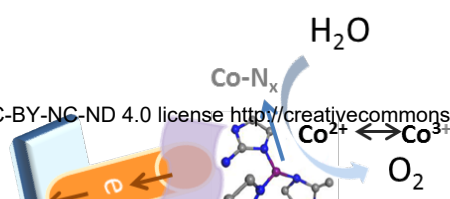
Scheme 1 Principle prcess of the PEC water oxidation on Co-MOF modified hematite photoanodes

Conclusions:

In summary, we have developed a facile method for in situ growth of Co-MOF on the surface of hematite photoanodes, which delivered an enhanced PEC activity toward water oxidation. Co $(NO_3)_2$ and 2-methylimidazole were used as precursors for growth of Co-MOF and varied Co/MIm ratios led to different morphologies. Under optimized conditions, the photocurrent density and the onset potential of the Co-MOF modified hematite showed a significant increase to 2.0 mAcm^{-2} at 1.23 V vs RHE and a cathodic shift of 180 mV, as relative to bare hematite. Compared with the bulk CoO or Co^{2+}, the atomically distributed Co^{2+} existing in Co-MOF exhibited excellent hole storage capability and charge transfer efficiency as evidenced by the high surface capacitance and extremely low surface charge transfer resistance. Moreover, the in-situ formed Co-MOF showed higher concentration of unsaturated Co-N$_x$ than that of powder formed ZIF-67, which facilitated O species chemisorption and accordingly acted as highly active centers for oxygen evolution. This work offers a facile and cost-effective method to prepare efficient photoanodes for PEC water oxidation.

Acknowledgements

1. Hisatomi, T., J. Kubota, and K. Domen, *Recent advances in semiconductors for photocatalytic and photoelectrochemical water splitting.* Chem Soc Rev, 2014. **43**(22): p. 7520-35.

2. Jiang, C., et al., *Photoelectrochemical devices for solar water splitting - materials and challenges.* Chemical Society reviews, 2017.

3. Kment, S., et al., *Photoanodes based on TiO_2 and alpha-Fe_2O_3 for solar water splitting - superior role of 1D nanoarchitectures and of combined heterostructures.* Chemical Society Reviews, 2017. **46**(12): p. 3716-3769.

4. Wheeler, D.A., et al., *Nanostructured hematite: synthesis, characterization, charge carrier dynamics, and photoelectrochemical properties.* Energy & Environmental Science, 2012. **5**(5): p. 6682-6702.

5. de Carvalho, W. and F. Souza, *Recent advances on solar water splitting using hematite nanorod film produced by purpose-built material methods.* Journal of materials research, 2014. **29**(1): p. 16-28.

6. Sivula, K., F. Le Formal, and M. Graetzel, *Solar water splitting: progress using hematite (alpha-Fe_2O_3) photoelectrodes.* Chemsuschem, 2011. **4**(4): p. 432-449.

7. Chen, Z.D., H.; Miller, E. , *Photoelectrochemical Water Splitting: Standards, Experimental Methods, and Protocols*. 2013, Berlin: Springer.

8. Lee, Y., et al., *Synthesis and Activities of Rutile IrO_2 and RuO_2 Nanoparticles for Oxygen Evolution in Acid and Alkaline Solutions.* Journal of Physical Chemistry Letters, 2012. **3**(3): p. 399-404.

9. Zhong, D.K., et al., *Photo-assisted electrodeposition of cobalt–phosphate (Co–Pi) catalyst on hematite photoanodes for solar water oxidation.* Energy & Environmental Science, 2011. **4**(5): p. 1759.

10. Zhong, D.K. and D.R. Gamelin, *Photoelectrochemical Water Oxidation by Cobalt Catalyst ("Co–Pi")/α-Fe2O3 Composite Photoanodes: Oxygen Evolution and Resolution of a Kinetic Bottleneck.* Journal of the American Chemical Society, 2010. **132**(12): p. 4202-4207.

11. Xu, Y.-F., et al., *Toward High Performance Photoelectrochemical Water Oxidation: Combined Effects of Ultrafine Cobalt Iron Oxide Nanoparticle.* Advanced Functional Materials, 2016. **26**(24): p. 4414-4421.

12. Chen, Z., et al., *Amorphous Cobalt Oxide Nanoparticles as Active Water-Oxidation Catalysts.* Chemcatchem, 2017. **9**(19): p. 3641-3645.

13. Malara, F., et al., *α-Fe2O3/NiOOH: An Effective Heterostructure for Photoelectrochemical Water Oxidation.* ACS Catalysis, 2015. **5**(9): p. 5292-5300.

14. Zhong, D.K. and D.R. Gamelin, *Photoelectrochemical Water Oxidation by Cobalt Catalyst ("Co-Pi")/alpha-Fe_2O_3 Composite Photoanodes: Oxygen Evolution and Resolution of a Kinetic Bottleneck.* Journal of the American Chemical Society, 2010. **132**(12): p. 4202-4207.

15. Zhong, D.K., et al., *Photo-assisted electrodeposition of cobalt-phosphate (Co-Pi) catalyst on hematite photoanodes for solar water oxidation.* Energy & Environmental Science, 2011. **4**(5): p. 1759-1764.

16. Du, C., et al., *Ultrathin CoOx-modified hematite with low onset potential for solar water*

oxidation. Physical Chemistry Chemical Physics, 2017. **19**(21): p. 14178-14184.

17. Li, S., et al., *Fabrication of metallic charge transfer channel between photoanode Ti/Fe2O3 and cocatalyst CoOx: an effective strategy for promoting photoelectrochemical water oxidation.* Journal of Materials Chemistry A, 2016. **4**(42): p. 16661-16669.

18. Qiao, B.T., et al., *Single-atom catalysis of CO oxidation using Pt-1/FeOx.* Nature Chemistry, 2011. **3**(8): p. 634-641.

19. Wang, S., et al., *Water oxidation electrocatalysis by a zeolitic imidazolate framework.* Nanoscale, 2014. **6**(17): p. 9930-9934.

20. Dou, S., et al., *Atomic-Scale CoOx Species in Metal-Organic Frameworks for Oxygen Evolution Reaction.* Advanced Functional Materials, 2017. **27**(36).

21. Saracco, G., et al., *Outer Co(ii) ions in Co-ZIF-67 reversibly adsorb oxygen from both gas phase and liquid water.* Physical Chemistry Chemical Physics, 2014. **16**(13): p. 6139-6145.

22. Tao, L., et al., *Creating coordinatively unsaturated metal sites in metal-organic-frameworks as efficient electrocatalysts for the oxygen evolution reaction: Insights into the active centers.* Nano Energy, 2017. **41**(Supplement C): p. 417-425.

23. Zhang, T., et al., *In-situ Growth of Ultrathin ZIF-67 Nanosheets on Conductive Ti@TiO2/CdS Substrate for High-efficient Electrochemical Catalysis.* Electrochimica Acta, 2016. **219**(Supplement C): p. 623-629.

24. Liu, Z.Q., et al., *ZnCo2O4 Quantum Dots Anchored on Nitrogen-Doped Carbon Nanotubes as Reversible Oxygen Reduction/Evolution Electrocatalysts.* Advanced Materials, 2016. **28**(19): p. 3777-3784.

25. Kaneti, Y.V., et al., *Fabrication of an MOF-derived heteroatom-doped Co/CoO/carbon hybrid with superior sodium storage performance for sodium-ion batteries.* Journal of Materials Chemistry A, 2017. **5**(29): p. 15356-15366.

26. Fu, Z., et al., *Surface treatment with Al3+on a Ti-doped α-Fe2O3nanorod array photoanode for efficient photoelectrochemical water splitting.* Journal of Materials Chemistry A, 2014. **2**(33): p. 13705.

27. Spray, R.L., K.J. McDonald, and K.-S. Choi, *Enhancing Photoresponse of Nanoparticulate alpha-Fe2O3 Electrodes by Surface Composition Tuning.* Journal of Physical Chemistry C, 2011. **115**(8): p. 3497-3506.

28. Klahr, B., et al., *Photoelectrochemical and impedance spectroscopic investigation of water oxidation with "Co-Pi"-coated hematite electrodes.* J Am Chem Soc, 2012. **134**(40): p. 16693-16700.

29. Carroll, G.M. and D.R. Gamelin, *Kinetic analysis of photoelectrochemical water oxidation by mesostructured Co-Pi/α-Fe2O3photoanodes.* J. Mater. Chem. A, 2016. **4**(8): p. 2986-2994.

30. Jiao, F. and H. Frei, *Nanostructured cobalt and manganese oxide clusters as efficient water oxidation catalysts.* Energy & Environmental Science, 2010. **3**(8): p. 1018-1027.

31. Jiao, F. and H. Frei, *Nanostructured Cobalt Oxide Clusters in Mesoporous Silica as Efficient Oxygen-Evolving Catalysts.* Angewandte Chemie-International Edition, 2009. **48**(10): p. 1841-1844.

32. Gerken, J.B., et al., *Electrochemical Water Oxidation with Cobalt-Based Electrocatalysts from pH 0-14: The Thermodynamic Basis for Catalyst Structure, Stability, and Activity.* Journal of the American Chemical Society, 2011. **133**(36): p. 14431-14442.

33. Qin, J., S. Wang, and X. Wang, *Visible-light reduction CO2 with dodecahedral zeolitic*

imidazolate framework ZIF-67 as an efficient co-catalyst. Applied Catalysis B-Environmental, 2017. **209**: p. 476-482.

34. Kaneti, Y.V., et al., *Fabrication of an MOF-derived heteroatom-doped Co/CoO/carbon hybrid with superior sodium storage performance for sodium-ion batteries.* Journal of Materials Chemistry A, 2017. **5**(29): p. 15356-15366.

35. Wang, S.H., et al., *Nanoparticle Cookies Derived from Metal-Organic Frameworks: Controlled Synthesis and Application in Anode Materials for Lithium-Ion Batteries.* Small, 2016. **12**(17): p. 2365-2375.

36. Rokicinska, A., et al., *Cobalt-containing BEA zeolite for catalytic combustion of toluene.* Applied Catalysis B-Environmental, 2017. **212**: p. 59-67.

37. Tang, Q.H., et al., *Characterizations of cobalt oxide nanoparticles within faujasite zeolites and the formation of metallic cobalt.* Chemistry of Materials, 2004. **16**(10): p. 1967-1976.

38. Klahr, B., et al., *Electrochemical and photoelectrochemical investigation of water oxidation with hematite electrodes.* Energy & Environmental Science, 2012. **5**(6): p. 7626-7636.

39. Hamann, T.W., *Splitting water with rust: hematite photoelectrochemistry.* Dalton Transactions, 2012. **41**(26): p. 7830-7834.

40. Zandi, O., B.M. Klahr, and T.W. Hamann, *Highly photoactive Ti-doped α-Fe$_2$O$_3$ thin film electrodes: resurrection of the dead layer.* Energy Environ. Sci., 2013. **6**(2): p. 634-642.

41. Pylypenko, S., et al., *Non-platinum oxygen reduction electrocatalysts based on pyrolyzed transition metal macrocycles.* Electrochimica Acta, 2008. **53**(27): p. 7875-7883.